Nanoscale Advances

ROYAL SOCIETY OF CHEMISTRY

MINIREVIEW

View Article Online
View Journal | View Issue

Cite this: *Nanoscale Adv.*, 2022, **4**, 2399

Organic ultrathin nanostructure arrays: materials, methods and applications

Yanjie Wei,†[a] Yue Geng,†[bc] Kui Wang,[a] Hanfei Gao,*[ab] Yuchen Wu [ab] and Lei Jiang [ab]

Organic ultrathin semiconductor nanostructures have attracted continuous attention in recent years owing to their excellent charge transport capability, favorable flexibility, solution-processability and adjustable photoelectric properties, providing opportunities for next-generation optoelectronic applications. For integrated electronics, organic ultrathin nanostructures need to be prepared as large-area patterns with precise alignment and high crystallinity to achieve organic electronic devices with high performance and high throughput. However, the fabrication of organic ultrathin nanostructure arrays still remains challenging due to uncontrollable growth along the height direction in solution processes. In this review, we first introduce the properties, assembly methods and applications of four typical organic ultrathin nanostructures, including small molecules, polymers, and other organic–inorganic hybrid materials. Five categories of representative solution-processing techniques for patterning organic micro- and nanostructures are summarized and discussed. Finally, challenges and perspectives in the controllable preparation of organic ultrathin arrays and potential applications are featured on the basis of their current development.

Received 13th December 2021
Accepted 20th April 2022

DOI: 10.1039/d1na00863c

rsc.li/nanoscale-advances

1. Introduction

Organic semiconducting materials have attracted wide attention in the fields of optoelectronics, and sensing and wearable devices, due to their low cost, flexibility, high charge transport efficiency and long carrier lifetime.[1–3] Compared to their traditional inorganic counterparts, organic crystals with large areas and high quality can be formed through solution processing due to dynamic and reversible noncovalent bonding interactions in organic molecules.[4] Furthermore, organic semiconductors with designable molecular structures, tunable band structures and programmable molecular stacking behavior could be synthesized by flexible arrangement of three bonding modes (including single, double and triple bonds) and introduction of diversified heteroatoms (such as nitrogen, oxygen, fluorine, silicon, phosphorus, sulfur, chlorine, selenium, bromine, iodine and even metallic elements).[5] Packing arrangements and crystal morphologies result in enormous differences in optoelectronic properties, which are greatly affected by molecular structures with different C/H ratios, substituents, and configurations. Therefore, organic molecules exhibit adjustable physical and chemical properties, including conductivity, photoelectricity, ferroelectricity, and catalytic activity and selectivity.[6–10]

Low-dimensional nanomaterials of semiconductors show many unprecedented properties that are unattainable in their counterparts, such as excellent mechanical strength, flexibility and high exposure of surface atoms, which are quite important for device applications.[11] Similarly, for organic semiconductors, the reduction of the semiconductor layer can minimize material consumption and provide remarkable opportunities for scaling down the devices to realize excellent short channel devices.[12] Organic ultrathin materials, especially, with the features of molecular level thickness, involve assembling organic low-dimensional nanostructures with long-range order. Owing to their small thickness, they could achieve various electronic, optical and chemical properties, including strong light-matter coupling, high optical transparency and highly exposed active surface.[13–15] Furthermore, decreasing the semiconductor thickness can inherently exclude the interlayer screening effect, which would provide great promise for high-performance optoelectronic properties.[16,17] At present, ultrathin nanostructures have been realized through designing various organic materials, such as small molecules, polymers, metal–organic frameworks (MOFs) and organic–inorganic hybrid perovskites. Their growth is accessible by two approaches: the introduction of strong epitaxial interactions and the use of molecules with intrinsic planar configuration, which provide high-performance in optoelectronics, catalysis and sensing. For

[a]*Ji Hua Laboratory, Foshan, Guangdong, 528200, P.R. China. E-mail: gaohanfei15@mails.ucas.ac.cn*

[b]*CAS Key Laboratory of Bio-inspired Materials and Interfacial Science, Technical Institute of Physics and Chemistry, Chinese Academy of Sciences, Beijing, 100190, P.R. China*

[c]*University of Chinese Academy of Sciences (UCAS), Beijing 100049, P. R. China*

† These authors have contributed equally to this work.

instance, the ultrathin active layer can reduce contact resistance in field effect transistors (FETs) and promote the realization of high transit frequency for organic FETs, which will better realize high-performance integrated devices.[18,19]

To achieve industrialization, fabrication of ultrathin organic arrays with a large area, precise alignment, high crystallinity and a tunable morphology is essential for the integration of organic electronic devices. Fabricating organic nanostructure arrays with a specific morphology can also realize the wide application of integrated devices, such as sensitive sensors,[20] logic computations[21] and multifunctional micro-nano lasers.[22] Recently, through patterning micro-droplets, an accurate control of the crystal position and morphology was realized by a series of techniques.[23,24] However, to date, the regulation of the crystallization process in most strategies is still limited, especially in the height direction of arrays. Combining the advantages of organic ultrathin nanostructures and well-patterned arrays is of great importance to the commercial development of integrated electronics and optoelectronics. Consequently, summarizing recent developments in organic ultrathin nanostructure arrays will boost development in this significant research area.

In this review, we highlight recent progress in organic ultrathin nanostructure arrays, including materials, methods and devices (Fig. 1). In the first part, the fabrication of organic ultrathin structures is introduced, involving several familiar organic molecules. Then, recent developments in strategies that have been developed for organic arrays are discussed and described with comments on their characteristics. Among them, we focus on the practical preparation method of organic ultrathin arrays. Finally, a summary of current challenges for organic ultrathin nanostructure arrays and their device applications is discussed together with their future perspectives.

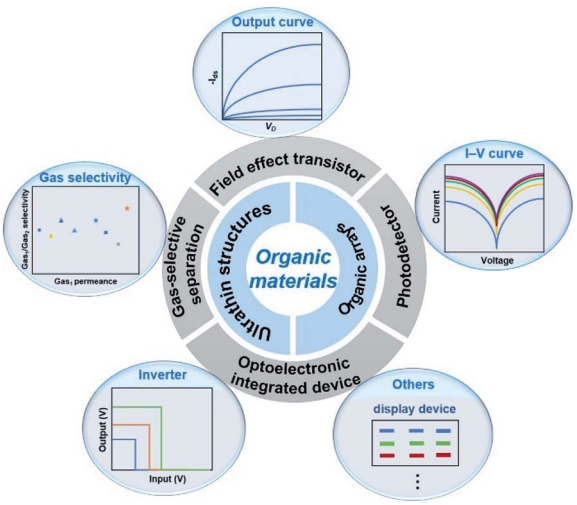

Fig. 1 Summary of ultrathin structures, array fabrication techniques, and their corresponding optoelectronic applications of organic materials.

2. Organic ultrathin materials

2.1. Properties of organic ultrathin materials

Organic ultrathin materials exhibit many promising and unprecedented physical and chemical properties owing to their small thickness, attracting significant research interest in a wide range of areas, including photonics, electronics, biosensing and catalysis.[15,18,25] First, the relative atomic thickness of tens or hundreds of nanometers endows organic ultrathin materials with excellent flexibility, optical transparency and ultimate scalability, which are crucial for the construction of next-generation novel applications.[26] Second, quantum confinement effects with limited lateral dimensions for organic ultrathin materials such as small molecules and organic–inorganic hybrid perovskites facilitate fascinating photonic and electronic properties; these materials are promising candidates for promising practical applications toward light-emitting diodes (LEDs),[27] FETs,[28] solar cells[29] and sensors.[30] Third, the large specific surface areas and ultrahigh lateral size of organic ultrathin materials render them good alternatives for surface-related applications such as photocatalysis,[31,32] electrocatalysis[33,34] and supercapacitors.[35]

2.2. Fabrication of ultrathin materials

2.2.1. Small molecules. Organic semiconducting small molecules are carbon-based π-bonded conjugated compounds, allowing charge conduction through the crystal in an applied electric field.[36] Unlike inorganic crystals with strong chemical bonds among atoms, these conjugated molecules with light weight, high tunability and excellent adaptivity are assembled *via* weak van der Waals forces (*e.g.* π–π interactions) ensuring a bright future with prospective multifunctionality for novel optoelectronics.[37] Compared with their bulk states, ultrathin organic semiconductor films composed of a single molecular layer or a small number of molecular layers could effectively alleviate interlayer screening, thus offering an appropriate system to directly exploit the effects of disorder and interfacial properties on charge transport.[38] Furthermore, both carrier injection and modulation become efficient to improve the performance of organic optoelectronics.[25]

Van der Waals epitaxy is suitable to precisely assemble organic small molecule semiconductors to realize many optoelectronic devices. This method takes advantage of the tunable van der Waals force between the substrate and small molecules to achieve layer-by-layer epitaxy of ultrathin semiconductors with a well-defined number of layers and self-limited characteristics at the liquid–solid, gas–solid, gas–liquid and liquid–liquid interface (Fig. 2a, d, g and j). Cao *et al.* grew a 1,4-bis(4-methylstyryl)benzene (*p*-MSB) two-dimensional (2D) single crystal on thermally oxidized SiO_2 on a Si substrate with controllable thickness. By using a seed-epitaxial drop casting technique, mono- or a few layers of 2D *p*-MSB crystal were obtained on the substrate.[39] Interestingly, the thickness of the first layer was different from the following layers, indicating a special packing mode with an immanent tilt angle of 9° for the interfacial *p*-MSB owing to its asymmetric molecular structure

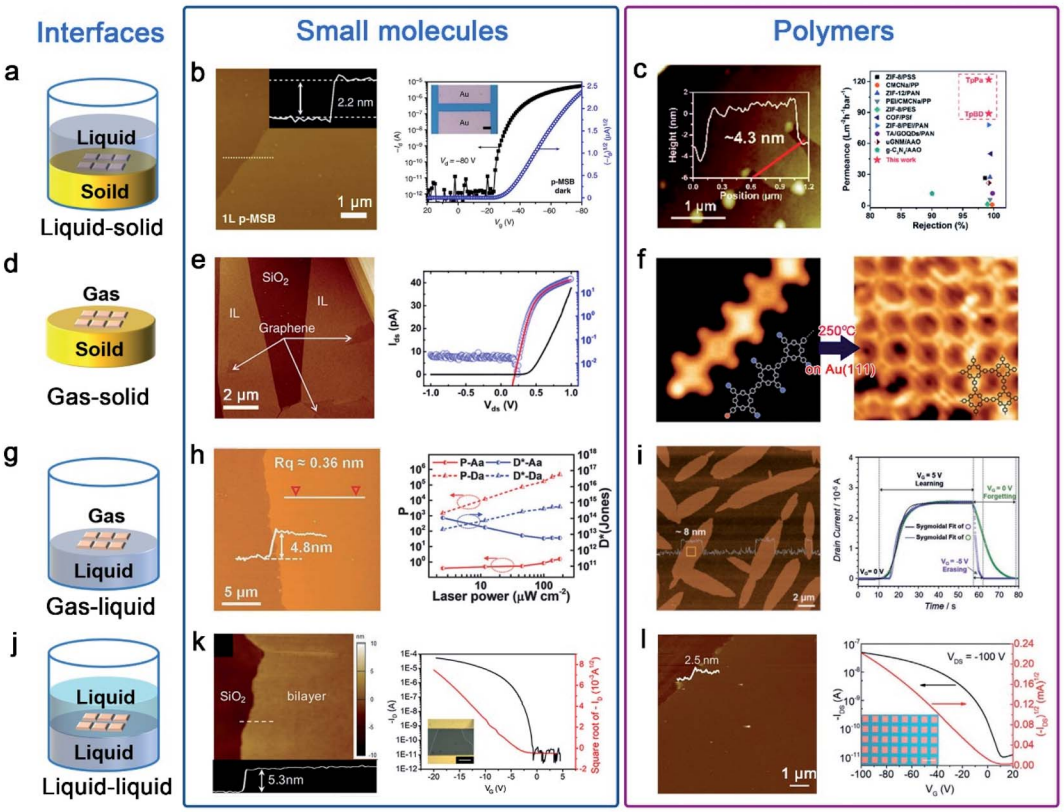

Fig. 2 Ultrathin nanostructures of small molecules and polymers are synthesized by the interface-induced epitaxial assembly method. (a) Schematic illustration of the liquid–solid interface. (b) AFM image of 1L *p*-MSB on SiO_2/Si; the insets show the corresponding height profile across the dashed lines. Transfer curve of a *p*-MSB FET device when the drain voltage is −80 V; the inset shows the optical microscopy image of the *p*-MSB FET device.[39] Adapted with permission from ref. 39. Copyright 2019, Springer Nature. (c) AFM image of the imine-linked 2D polymers named TpBD and the membranes with excellent rejection rates and remarkably high water permeances.[51] Adapted with permission from ref. 51. Copyright 2020, Royal Society of Chemistry. (d) Schematic illustration of the gas–solid interface. (e) AFM image of the 1L C8-BTBT film on graphene and output characteristics of the PTCDA/C8-BTBT heterojunction.[41,42] Adapted with permission from ref. 41. Copyright 2014, Springer Nature. Adapted with permission from ref. 42. Copyright 2016, American Chemical Society. (f) STM images of molecules on Au(111): 2D polymers appear after heating the sample to 250 °C.[53] Adapted with permission from ref. 53. Copyright 2012, Springer Nature. (g) Schematic illustration of the gas–liquid interface. (h) AFM image of the 2D TFT-CN film and the P and D* of the phototransistors as a function of the incident light intensity.[44] Adapted with permission from ref. 44. Copyright 2018, John Wiley and Sons. (i) AFM image of the 2D BECOF-PP film on a Si/SiO_2 substrate and learn-erase/learn-forget cycles of the 2D BECOF-PP/SiNW hybrid device.[56] Adapted with permission from ref. 56. Copyright 2020, John Wiley and Sons. (j) Schematic illustration of the liquid–liquid interface. (k) AFM image of bilayer C8-BTBT on a SiO_2/Si substrate. Transfer characteristics at a drain voltage of −20 V; the inset shows the optical microscopy image of the 2D C8-BTBT FET.[47] Adapted with permission from ref. 47. Copyright 2016, John Wiley and Sons. (l) AFM image of the 2DPTTI film and representative transfer curves of 2DPTTI-based transistors.[58] Adapted with permission from ref. 58. Copyright 2020, John Wiley and Sons.

(Fig. 2b). Furthermore, the authors successfully applied the *p*-MSB 2D crystal onto a planar p-type FET with an on/off ratio up to ~10^6 and a high mobility of 0.226 $cm^2\ V^{-1}\ s^{-1}$. The linear output curves at low V_d indicate excellent charge injection.

Wang *et al.* demonstrated that high-quality ultrathin films of organic small molecules, such as dioctylbenzothiophene (C8-BTBT) and pentacene, can be grown on a graphene or boron nitride substrate *via* solid–gas interface van der Waals epitaxy, with precisely controlled thickness down to monolayer, large-area single crystals, simple preparation and patterning capability.[40–42] The C8-BTBT film is epitaxially grown on graphene through physical vapor transport, where the C8-BTBT-substrate binding energy (BE) depends on the substrate. Fig. 2e shows an atomic force microscope (AFM) snapshot of the C8-BTBT film during epitaxy growth. The crystals preferentially grew on graphene, in a layer-by-layer fashion with atomic smoothness. Planar OFETs based on epitaxial C8-BTBT crystals on insulating BN with a monolayer thickness (~1.7 nm) exhibit several features of ideal OFETs with linear $I_{ds}^{1/2}$–V_g characteristics in the linear (saturation) regime and negligible hysteresis. μ at room temperature could reach up to ~10 $cm^2\ V^{-1}\ s^{-1}$, higher than previously reported values for monolayer OFETs (in the range of ~10^{-6}–0.1 $cm^2\ V^{-1}\ s^{-1}$). This technique can also be applied to build a graphene/(perylene-3,4,9,10-tetracarboxylic dianhydride)PTCDA/C8-BTBT/Au heterojunctions, showing excellent rectifying *I*–*V* characteristics with a rectifying ratio over 1000 at room temperature. The *I*–*V* characteristics were described by a standard diode model with a series resistance. The derived factor of 1.27 confirms the presence of a nearly ideal heterointerface.

Recently, Hu's Group developed a facile and general method named "solution epitaxy" to grow 2D crystals of organic semiconducting small molecules at the water–air interface.[43] Wang *et al.* successfully prepared millimeter-sized 2D crystal films of n-type organic semiconductors (a furan-thiophene quinoidal compound, TFT-CN) on the surface of water; their thickness is below 5 nm (Fig. 2h).[44] An outstanding field-effect electron mobility and high on/off ratio based on TFT-CN were obtained in air. Meanwhile, ultrasensitive near-infrared organic phototransistors were also obtained; the photocurrent on/off ratio and detectivity can reach $\approx 5 \times 10^5$ and 6×10^4 Jones attributed to low dark current $I_d \approx 0.3$ pA. Zhu *et al.* reported high-performance and well-balanced ambipolar OFETs; TFT-CN and 2,6-bis(4-hexylphenyl)anthracene (C6-DPA) grown on the water surface were used as the p-type and n-type architype semiconductors, respectively.[45] Subsequently, Yao *et al.* replaced water with high-viscosity glycerin and large-area quasi-free-standing 2D small molecule crystals from the bulk down to the monolayer limit were prepared.[46]

A liquid–liquid interface was also employed for the epitaxial growth of organic semiconductor molecules. For example, Hu *et al.* employed an ideal water–oil epitaxy interface to fabricate large area and high quality organic ultrathin crystals.[13] Wang *et al.* also assembled C8-BTBT molecules into precisely ultrathin layer-defined structures in a mixture solvent of anisole and immiscible *p*-anisaldehyde.[47] The mixture solution was drop-cast onto the SiO_2/Si substrate, and a mechanical pump generated an airflow on top of the droplet, dragging the droplet to move at a speed of ≈ 6 mm s^{-1}. Near the solution edge, the evaporation-driven flow of the good solvent leads to a coffee-ring effect on the antisolvent, providing a defined location for the crystallization of C8-BTBT molecules with a high crystal growth rate. With solution edge sliding, C8-BTBT films with 2D material features were formed immediately. The exposed monolayer C8-BTBT generally consists of small patches in sub-micrometre sizes and the bilayer C8-BTBT exhibits uniform thin films with a thickness of approximately 5.3 nm (Fig. 2k). The transfer characteristics of the device with the bilayer C8-BTBT result in a high field-effect μ of 5.2 $cm^2 V^{-1} s^{-1}$. The device also yields a high on/off ratio of 10^6, a near-zero threshold voltage (V_{th}) ~3 V, and a low subthreshold swing of 0.4 V dec^{-1}.

2.2.2. Polymers. Polymers are organic semiconductors in that they are carbon-based systems with extended conjugation along the polymer backbone. This class of materials comprises repeated units of conjugated monomers, with tunable optoelectronic properties based on the monomer molecular structure. 2D polymers that are laterally infinite, one atom- or monomer-unit thin, free-standing, covalent networks with long-range order along two orthogonal directions have attracted intense attention in recent years due to their wide application in electronics, membranes and sensing.[48–50]

Similar to small molecules, the rational design of well oriented ultrathin polymer nanostructures nowadays mainly focuses on interface-induced epitaxial assembly (Fig. 2a, d, g and j). Through liquid–solid interface reactions, Shi *et al.* presented an exfoliation-free approach for preparing few-layered 2D polymer nanosheets.[51] NaCl particles as sacrificial substrates were added into the reaction system to create billions of solid–liquid interfaces. By adjusting salt sizes and growth conditions, polymerization was exclusively confined to salt surfaces leading to yield large numbers of ultrathin nanosheets with the thickness down to a few nanometers. As shown in Fig. 2c, the imine-linked 2D polymers named TpBD with thicknesses ~4.3 nm were prepared; the membranes based on these thus-obtained 2D polymers exhibit remarkably high water permeances and tight selectivity much higher than that of other membranes.

The gas–solid interface is also employed to fabricate ordered 2D polymer nanostructures. In this field, reactions are typically conducted in an ultrahigh vacuum within the cavity of a scanning tunneling microscope (STM); flat heating metal crystal substrates such as Au, Cu and Ag are widely used.[13] Inspired by the Ullmann coupling reaction, Grill *et al.* first reported in 2007 that covalently bound molecular nanostructures can be formed on a gold surface.[52] In order to improve the quality of 2D polymers, they also developed a sequential growth strategy by the selective and activation of specific sites.[53] Due to different reactivities, linear chains of porphyrin molecules were created on heating to 120 °C and then 2D architectures were formed after heating to 250 °C on Au(111) (Fig. 2f). Although the gas–solid interface strategy has made considerable progress, strict reaction conditions and low surface coverage greatly limit their further applications.

In comparison with the gas–solid interface, the gas–liquid interface is more favorable for synthesizing 2D polymer nanosheets because it does not require complex reaction conditions and expensive equipment. Moreover, it can provide an atomically flat surface on a large scale and dynamic reaction environment to produce large-area 2D polymer nanosheets. Recently, Wang *et al.* reported the preparation of self-assembled ultrathin polydopamine (PDA) films at an air–water interface.[54] In the last three years, Feng's Group had also reported some studies of synthesizing 2D polymers on the water surface.[55–57] For example, they reported the synthesis of crystalline 2D polyimine films by employing a surfactant-monolayer-assisted interfacial synthesis (SMAIS) at the gas–liquid interface.[56] As show in Fig. 2i, few-layer 2D boronate ester covalent organic framework (BECOF) films composed of porphyrin macrocycles and phenyl (2D BECOF-PP) were obtained. A bio-inspired system to mimic neuronal synapses composed of 2D BECOF-PP films on a silicon nanowire-based field-effect transistor was built, and displayed a learning-erasing-forgetting memory process.

A liquid–liquid interface comprising two immiscible solvents can also provide a confined reaction zone for the construction of 2D polymer nanosheets. Due to the fluidity of liquid, large-area monolayer 2D polymer nanosheets can be obtained by the liquid–liquid interface strategy. One typical example is to synthesize 2D polytriethyltriindole (2DPTTI) through a Suzuki reaction between 2,7,12-tribromo-5,10,15-triethyltriindole (2-BrTTI) and 1,4-benzenediboronic acid dipinacol ester (BADE) monomers at a toluene–water interface at room temperature, which was reported by Li *et al.* in 2020.[58] By adjusting the experimental conditions, the obtained 2DPTTI film thickness can be scaled down to 2.5 nm and the films exhibited typical p-type transporting performance (Fig. 2l).

Except for immiscible organic–aqueous interfaces, Li *et al.* reported the first example of growing 2D polymer nanosheets at the interface of two miscible organic solvents.[59] By adding a low-density solvent interlayer as a buffer layer between two miscible solvents, super-large size and high-quality 2D nanosheets with a smooth surface were obtained.

2.2.3. MOFs. MOFs constructed by coordination bonds between metal ions or clusters and organic ligands have emerged as a class of porous materials and drawn tremendous attention.[60,61] Compared to traditional bulk MOF crystals, ultrathin MOF nanostructures are receiving broad research interest because of their structural diversity, rich catalytic active sites and larger surface area.[62,63]

To date, many efficient synthetic methods have been developed to synthesize ultrathin MOF nanostructures. In general, all synthesis methods can be classified as top–down and bottom–up methods (Fig. 3a and b).[64] The top–down method, mainly containing sonication exfoliation, mechanical exfoliation and chemical exfoliation, is a processing method which exfoliates layered bulk MOFs into monolayer or few layers materials.[65] The coordinate bond in bulk MOFs is much stronger than the weak interaction between neighboring layers; based on this, the key principle of the top–down method is resorting to either the external forces to directly break the weak interactions (*i.e.* van der Waals forces or π–π stacking) or the introduction of intercalated molecules to weaken the interactions. In contrast, the bottom–up approach is a self-assembly method for directly obtaining ultrathin MOFs by assembly of metal ions and organic ligands. For obtaining ultrathin MOFs, the major technical challenge is how to promote growth in the lateral direction while arresting in the vertical direction. As shown in Fig. 3b, the foremost synthesis methods of ultrathin MOFs include interfacial synthesis, modulated-assisted synthesis and surfactant-assisted synthesis.[64,66] Interfacial synthesis is broadly applied to prepare ultrathin MOFs by the reaction of metal ions and organic ligands at the confined interface, including the gas/liquid interface, liquid/liquid interface and liquid/solid interface. Modulated-assisted synthesis is also usually employed in the production of ultrathin MOFs. Modulators with surfactants and small molecules can selectively adsorb on the surface of

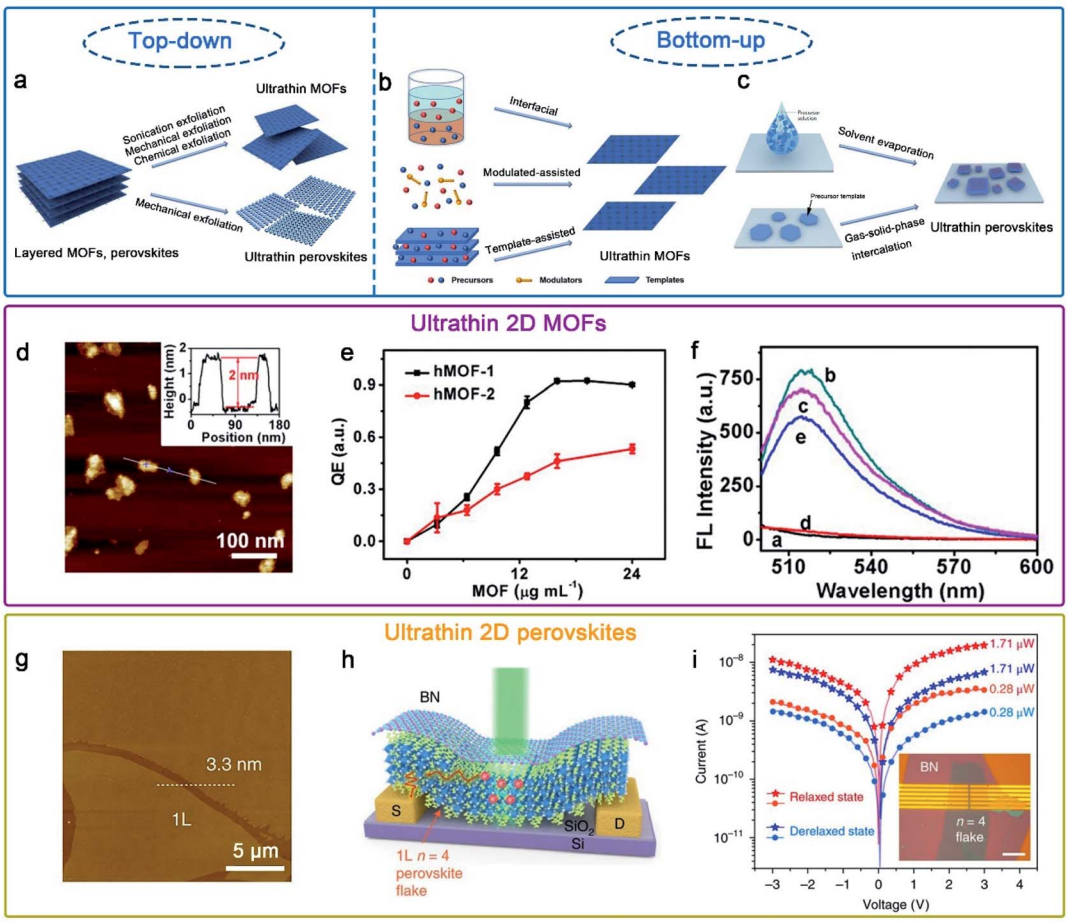

Fig. 3 Schematic illustration of the preparation of (a) ultrathin MOFs and perovskites by top–down methods, and (b) ultrathin MOFs and (c) perovskites by bottom–up methods.[64,80] Adapted with permission from ref. 64. Copyright 2020, Springer Nature. Adapted with permission from ref. 80. Copyright 2020, Springer Nature. (d)–(f) hMOF-1 nanosheet-based axial coordination platform for DNA detection.[70] Adapted with permission from ref. 70. Copyright 2019, American Chemical Society. (g)–(i) $(C_4H_9NH_3)_2(CH_3NH_3)_3Pb_4I_{13}$ ($n = 4$) perovskite photodetector device fabricated on exfoliated monolayer flakes.[77] Adapted with permission from ref. 77. Copyright 2018, Springer Nature.

metal nodes or coordinate competitively with metal nodes to regulate the lateral direction growth of MOFs. Template-assisted synthesis is a kind of physical confining method, which refers to the introduction of appropriate templates in producing ultrathin MOFs.

Due to the unique physical and chemical properties of ultrathin MOFs, they have widespread application prospects in many fields, such as sensing,[67] gas separation[68] and catalysis.[69] For instance, Wong *et al.* obtained easily Hofmann-type MOF (hMOF) monolayer nanosheets *via* a top–down method (Fig. 3d–f),[70] and hMOF nanosheets as an axial coordination platform for DNA detection exhibited excellent quenching ability to fluorophores *via* a ligand-to-metal charge-transfer mechanism.

2.2.4. Organic–inorganic hybrid perovskites. Organic–inorganic hybrid perovskites have received considerable research attention as a prospective semiconductor due to their unique excitonic properties and impressively high performance in photovoltaics and optoelectronic devices.[71–73] Beyond three-dimensional (3D) hybrid perovskites, the newly emerging 2D Ruddlesden–Popper perovskites (RPPs) as representative examples of layered materials have received increasing attention due to their better environmental stability.[74] It is understood that ultrathin nanostructures exhibit unique features compared to their corresponding bulk counterparts.[75,76] Therefore, the controllable preparation of ultrathin perovskites has attracted growing attention and is of great significance for high-performance optoelectronic devices.

To date, several practical methods have been used for the preparation of ultrathin hybrid perovskites. On account of their van der Waals stacked structure, 2D RPPs can be exfoliated down to few and single layers *via* mechanical or chemical exfoliation (Fig. 3a).[77,78] Besides, the solution-phase method has been developed and widely used *via* solvent evaporation (Fig. 3c).[79,80] Epitaxial growth is a two-step method using a combined solution process and vapor-phase conversion method to grow ultrathin 2D hybrid perovskite with spatial precision and adjustable thickness (Fig. 3c). In previous reports, the controlled 2D PbI_2 was prepared as the template, and then ultrathin 2D $CH_3NH_3PbI_3$ perovskite nanocrystals were successfully prepared through gas–solid-phase intercalation of CH_3NH_3I molecules.[75]

Hybrid perovskites with a few-unit-cell or molecular-scale thickness allows better gate electrostatics and more efficient carrier extraction when they are used as photodetectors.[80,81] Recently, Leng *et al.* synthesized large-sized crystals of $(CH_3(-CH_2NH_3(CH_3NH_3)_{n-1}Pb_n)_3)_2I_{3n+1}$ ($n = 1, 2, 3, 4$); subsequently, large-sized monolayers were obtained mechanically exfoliated from the corresponding bulk single crystals.[77] Moreover, a highly efficient photodetector was fabricated using a molecularly thin $n = 4$ RPP crystal, possessing a high responsivity and detectivity value (Fig. 3g–i).

3. Organic nanostructure arrays

3.1. Advantages of organic arrays

Organic arrays are the most ideal and indispensable building units for large-scale and high-performance organic photonic and electronic circuits, as well as the key substructure for the fabrication of novel and ultra-efficient optoelectronics devices. Organic one-dimensional (1D) arrays can not only function as component devices, but also as irreparable connections between each device unit, owing to their significant advantages in geometry control, mechanical flexibility and solution processability.[82,83] Remarkably, long-range order and high crystallinity organic 1D architectures exhibit suppressed grain boundaries, long carrier transport ability and high-performance stability, which have been validated to enhance optical and electrical performance and push the realm of flexible photonics/electronics forward. However, the assembly of high-quality organic arrays especially for ultrathin arrays faces many challenges, such as indeterministic alignment, poor-quality crystallography and limitation of material lateral dimensions. Currently, methods for fabricating organic arrays can be divided into two categories: physical vapour transport (PVT) strategies and solution-processing techniques. It is necessary to point out that the traditional PVT method use patterned nanoseeds to target organic semiconductors, but there are challenges in the fabrication of 1D and more complex patterned structures.[84–86] In the follow-up, some modified PVT methods have also been developed to control the growth of organic nanostructures, such as a guided PVT technique by pillar-structured substrates.[87] Compared with PVT strategies, solution-processing techniques are more flexible and practical. In recent decades, many techniques including droplet-pinning,[88–91] inkjet printing,[17,92] nanoimprinting lithography,[93,94] dip-pen nanolithography,[95,96] solution shearing[21,97,98] and capillary-bridge lithography[99,100] have been developed to achieve the scale-up and controllable preparation of organic nanostructure arrays with integrated functions. In this section, we highlight and introduce five main solution-processing patterning strategies for fabricating organic architectures.

3.2. Solution processes for patterning

3.2.1. Inkjet printing. Inkjet printing is a typical direct writing method (Fig. 4a), which precisely deposits different organic micro and nanomaterials into integrated multifunctional patterns in a non-contact, maskless and cost-effective technique, has received considerable attention in recent years.[101–103] For example, Li *et al.* realized matrix green LEDs from a stable $FA_{0.3}Cs_{0.7}PbBr_3$ perovskite quantum dot (PeQD) ink with optimized octane by using the inkjet printing technique, as show in Fig. 4b, which may suggest a possibility of making perovskite quantum dot displays by using this technique.[104] Fang *et al.* fabricated patterned liquid crystalline (LC) films *via* inkjet printing for achieving high-performance organic integrated circuits.[105] The patterned C8-BTBT LC film-based 7×7 OFET array was realized, which has 100% die yield and shows a maximum mobility up to 9.33 $cm^2\ V^{-1}\ s^{-1}$ (Fig. 4c and d).

3.2.2. Nanoimprinting lithography. Nanoimprinting lithography (NIL) offers a simple and rapid replication process by transferring a uniform and precise nanoscale pattern shape of a mold on the surface, followed by removal of the mold (Fig. 4e).[93,106,107] The obtained patterns can be as small as sub 10

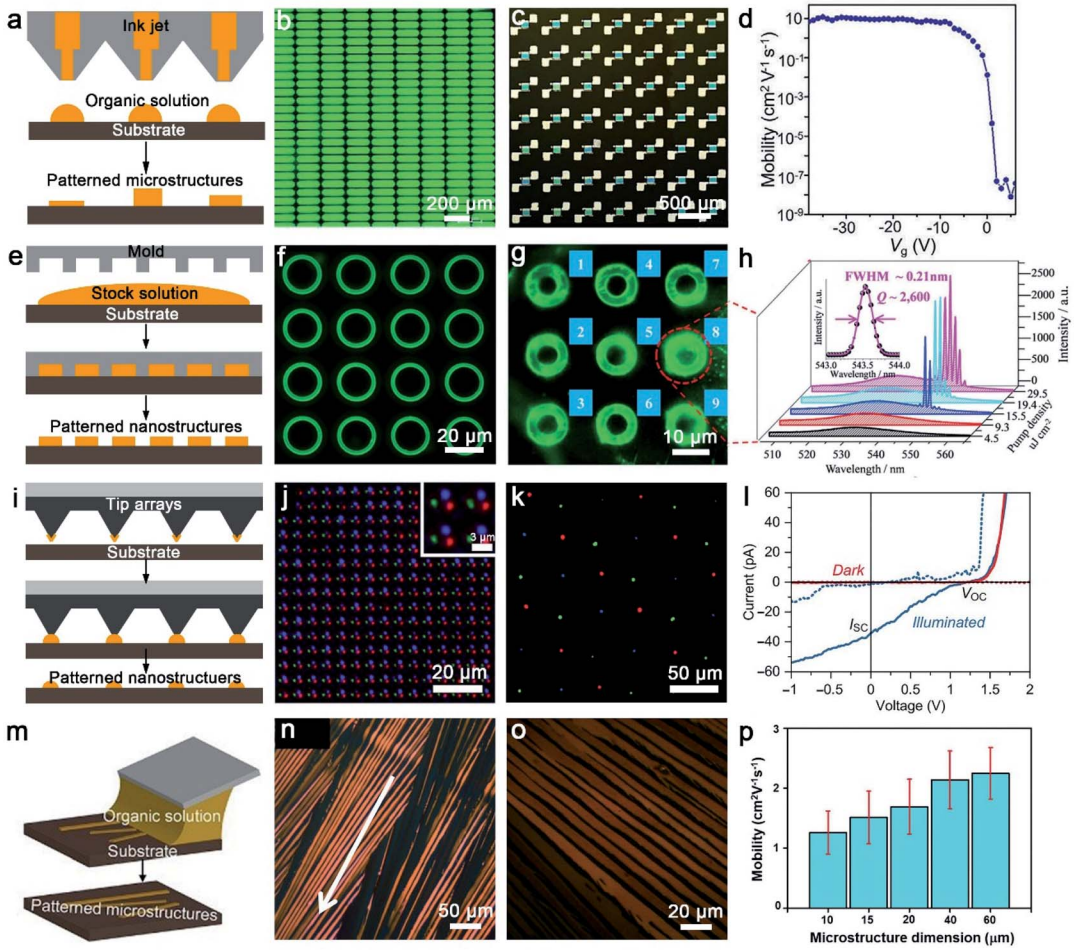

Fig. 4 (a) The schematic diagram of inkjet printing. (b) Light-on image of inkjet-printed matrix PeQD-LEDs with a bias of 4 V.[104] Adapted with permission from ref. 104. Copyright 2020, John Wiley and Sons. (c) and (d) Polarized optical microscope (POM) image of the patterned C8-BTBT LC film-based 7 × 7 OFET array and extracted mobility as a function of V_g.[105] Adapted with permission from ref. 105. Copyright 2021, John Wiley and Sons. (e) The schematic diagram of nanoimprint lithography. (f) Low-magnification μ-PL image of $\langle n \rangle = 6$ RPP microring arrays, (g) μ-PL image recorded above the lasing threshold, (h) spatially resolved μ-PL spectra recorded from microring 8 labeled in (g) as a function of P.[111] Adapted with permission from ref. 111. Copyright 2018, John Wiley and Sons. (i) The schematic diagram of dip-pen nanolithography. (j) The overlay fluorescence image presents the distribution of Oregon Green 488 WGA and AMCA rabbit anti-goat IgG (H + L) and spots printed sequentially with PPL along the substrate.[117] Adapted with permission from ref. 117. Copyright 2017, John Wiley and Sons. (k) Merged-channel confocal fluorescence image of tricolor nanocrystal pixel arrays composed of $MAPbI_3$ (red), $MAPbBr_3$ (green), and $MAPb(Br_{0.4}Cl_{0.6})_3$ (blue) with PPL, (l) current–voltage curves for a $MAPbBr_3$ nanocrystal in the dark (red) or illumined by a 455 nm LED light of ~3.6 mW cm^{-2} (blue).[118] Adapted with permission from ref. 118. Copyright 2017, Advancement of Science. (m) The schematic diagram of solution shearing. (n) Cross-POM image of solution-sheared TIPS-pentacene thin films, formed with a shearing speed of 1.6 mm s^{-1}.[119] Adapted with permission from ref. 119. Copyright 2011, Springer Nature. (o) Cross-POM image of TIPS-pentacene thin films solution-sheared using an AHPCS shearing blade with a microstructure dimension of 10 μm, and (p) comparison of the average mobility of FET solution-sheared with different microstructure dimensions.[124] Adapted with permission from ref. 124. Copyright 2018, John Wiley and Sons.

nm, which retains the nanoscale resolution of the mold.[94] In the past few decades, NIL has evolved into a series of methods to reduce the harsh conditions and achieve larger pattern areas, including UV-curable NIL, thermal NIL, laser-assisted NIL and room-temperature NIL.[94,108,109] Recently, Oh *et al.* developed scalable, simple, and inexpensive dissolvable template nanoimprinting lithography (DT-NIL).[110] They replicated cicada wings which have surface nanofeatures of ~100 nm in height by using the DT-NIL method, which demonstrates that the method can achieve scalable replication of a range of natural and engineered surfaces with complex surface topographies. In addition to the rigid mold, an elastomeric stamp with nanoscale patterns can be used as the soft mold of the NIL. Zhang *et al.* fabricated high-density large-area RPP microring laser arrays with a well-controlled size and shape by using a facile polydimethylsiloxane (PDMS) template-confined solution growth method (Fig. 4f–h).[111] The obtained lasing spectra were almost identical to different microrings, accompanied by a similar low lasing threshold and high-quality factor ($Q \approx 2600$).

3.2.3. Dip-pen lithography. Dip-pen nanolithography (DPN), invented by Mirkin's Group in 1999, is a novel scanning probe-based technique that can be used to write "inks" directly

on an underlying substrate.[112] In simple terms, DPN is fundamentally a patterning process which utilizes AFM tips for material transport; "inks" are then transferred from the tip to the substrate by physical or chemical adsorption (Fig. 4i). Thus, it has imparted this technology good compatibility with various soft and hard materials, opening up more possible applications.[113,114] In particular, to enhance DPN parallelization for high throughput, polymer pen lithography (PPL) was proposed based on a novel "cantilever-free" printing concept, which contains the advantages of cantilever-based DPN and microcontact printing.[115,116] Agusil *et al.* selectively printed different biomolecule patterns onto functionalized substrates for fabricating highly anisotropic suspended planar-array chips by using PPL, as presented in Fig. 4j.[117] Meanwhile, using the PPL technique with high resolution and high spot density increases the miniaturization of chips by two orders of magnitude compared to other fabrication methods, which presents a cornerstone for accurate bioanalysis. Du *et al.* reported a novel method of using PPL to synthesize compositionally diverse halide perovskite nanocrystal arrays spanning square centimeter areas.[118] The synthetic nanocrystalline arrays can construct RGB pixels and miniaturized solar cells based on single nanocrystals (Fig. 4k and l), which potentially paves the way toward the development of optoelectronic devices, such as multicolor optical displays and light-harvesting devices.

3.2.4. Solution shearing. Solution shearing, first introduced by Bao's Group,[119,120] is also proposed as an effective patterning method for producing aligned organic crystals over a large area. In this method, an organic semiconductor solution droplet is confined between a movable top shearing blade and a temperature-controlled substrate, as shown in Fig. 4m. By moving the blade at a fixed speed relative to the substrate, only the evaporation front of the solution is exposed, and aligned organic crystals along the shearing direction were deposited.[121,122] Due to the kinetic properties of the method, Bao's Group observed metastable molecular packing motifs in ribbon-like 6,13-bis(triisopropylsilylethynyl)pentacene (TIPS-pentacene) by using this method (Fig. 4n), which greatly enhanced charge transport as a result of the change of the intermolecular π–π stacking distance.[119] Apart from a rigid blade, through modifying solution shear technology, plastic materials were exploited instead of rigid materials.[123] In particular, Kim *et al.* introduced the use of allylhybridpolycarbosilane (AHPCS), an inorganic polymer, for solution shearing as the microstructured blade, which has good stability in various organic solvents, can be microstructured *via* using a simple soft-lithography process, and has high mechanical flexibility and durability.[124] TIPS-pentacene thin films solution-sheared using an AHPCS shearing blade with a microstructure dimension of 20 μm are shown in Fig. 4o. The average mobility of field-effect transistors solution-sheared with different microstructure dimensions are shown in Fig. 4p, which shows an increasing trend in field effect mobility with increasing microstructure dimensions.

3.2.5. Capillary-bridge lithography. To control the dewetting process of organic liquids, our group developed a universal capillary bridge lithography method to fabricate micro/nanoarrays based on various materials, including organic small molecules,[22,99] polymers,[125,126] metal-halide perovskites[127,128] and colloid nanoparticles,[129,130] by employing asymmetric-wettability topographical templates with lyophilic top and lyophobic sidewalls (Fig. 5a). The receding of the triphase contact line (TCL) in the dewetting process is strictly modulated by asymmetric-wettability micropillars, forming individual capillary bridges pinned onto the tops of micropillars. These discrete capillary bridge arrays provide a confined space for the controlled nucleation and growth of organic microcrystals. Fig. 5b presents a fluorescence microscopy image of organic 1D arrays, demonstrating high-quality and large-area organic architectures with a homogenous size and precise position. Furthermore, the TEM image in Fig. 5c exhibits the high-crystallinity nature and the [010] growth direction of organic 1D crystals.[99] Also by utilizing this assembly method, we fabricated 2D-perovskite single-crystalline nanowire arrays with a pure (101) crystallographic orientation, which possessed high resistance in the interior but high photoconductivity at edges.[20] Benefitting from these single-crystalline perovskite nanowires, ultrasensitive photodetectors with peak responsivities exceeding 1.5×10^4 A W^{-1} and detectivities exceeding 7×10^{15} Jones were demonstrated (Fig. 5d), which are remarkably higher than previous reports. A Stokes photodetector based on single-crystalline nanowires of chiral 2D perovskites fabricated by this method integrates linearly polarized and circularly polarized light detection, simultaneously.[131] The single-crystallinity and pure crystallographic orientation of 2D-perovskite nanowires permitted highly efficient carrier transport within the 1D structure, resulting in a responsivity of 47.1 A W^{-1} and a detectivity of 1.24×10^{13} Jones (Fig. 5e). Progress in the development of near-infrared (NIR) lasers based on organic materials is severely restrained by the difficult formation of a high-efficiency four-level energy system and low stimulated emission owing to intrinsic quenching transition in the NIR region.[132] Therefore, in our work, we first reported the multimode lasing emission at 775 nm based on organic single-crystalline nanowire arrays with the length of 70 μm. Fig. 5f exhibits the PL spectra at increasing pump densities with a narrow spacing $\Delta\lambda$ of 0.6 nm, indicating the well-performing lasing performance of our as-assembled organic 1D arrays. Conventional optical vapor sensors with solvatochromic shift mechanisms suffer from the risk of lower sensitivity due to weak interactions. Thus, we combined aggregation-induced emission (AIE) molecules with polymers to form a polymer/AIE arrays as a vapor sensor to mitigate this issue (Fig. 5g). The as-fabricated polymer/AIE microwires realized the successful classification and identification of different organic vapors with good stability and reproducibility.[133] Our research paves the way for the realization of multifunctional optoelectronic devices and the integration of organic photonic circuits.

To assemble high-quality organic ultrathin structures, we employed pressure between the periodically arranged micropillars and flat substrate to further manipulate this capillary-bridge-mediated assembly.[134] The nano-confined space between micropillars' tops and the substrate suppress the vertical growth of organic crystals, whereas the growth of crystals

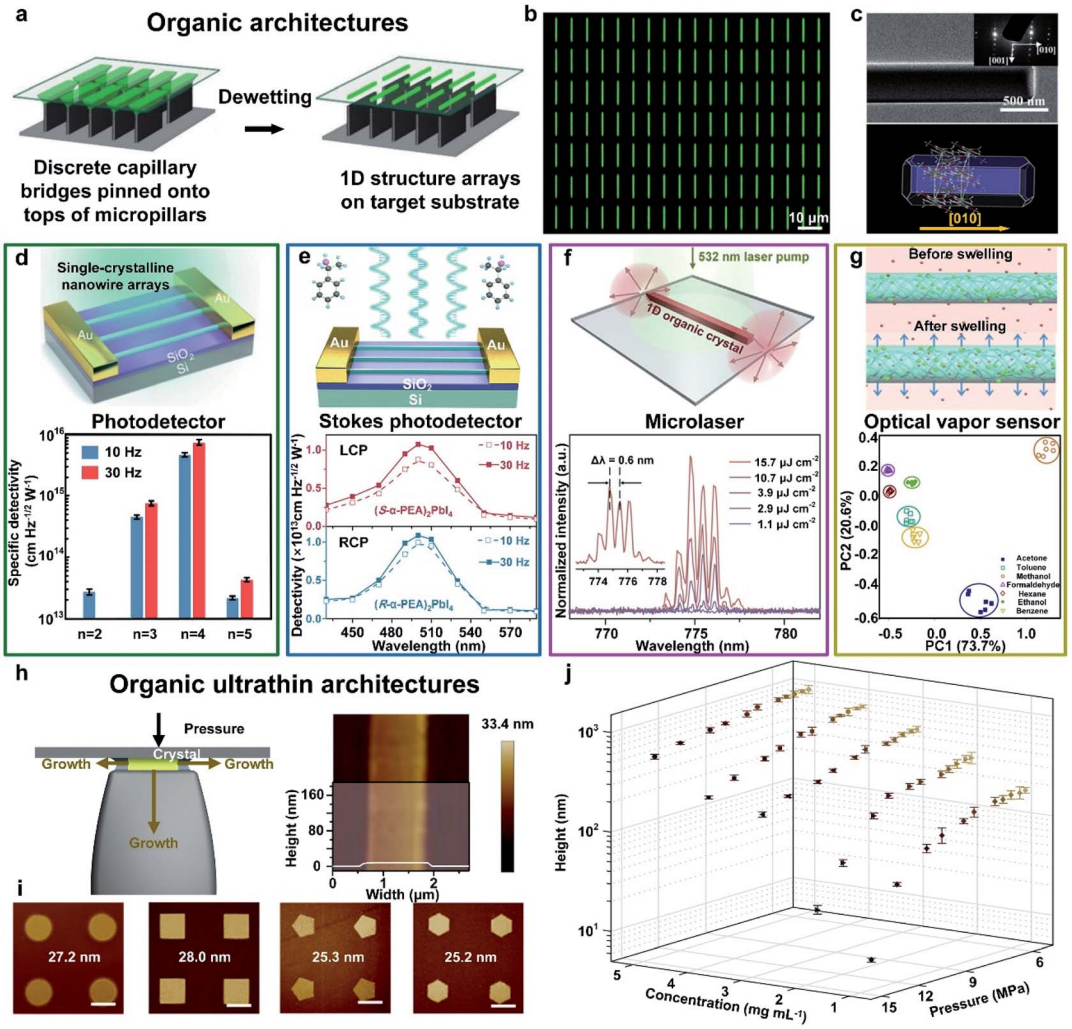

Fig. 5 Fabrication of organic architectures utilizing a capillary bridge lithography assembly system. (a) Schematic illustration of the dewetting process of organic 1D structure arrays on the micropillar-structured template with asymmetric-wettability. (b) and (c) The morphology and crystallization of organic arrays present high-quality 1D crystals with strict alignment, a precise position and single-crystalline nature.[99] Adapted with permission from ref. 99. Copyright 2017, John Wiley and Sons. (d) Fabrication of 2D perovskite nanowire photodetectors. Statistics of specific detectivities of $n = 2$–5 nanowires at modulation frequencies of 10 Hz and 30 Hz, respectively.[20] Adapted with permission from ref. 20. Copyright 2018, Springer Nature. (e) Fabrication of chiral 2D-perovskite Stokes photodetectors, which integrating linearly and circularly polarized light detection simultaneously. Wavelength-dependent detectivities of 2D perovskite nanowire photodetectors.[131] Adapted with permission from ref. 131. Copyright 2021, American Chemical Society. (f) Fabrication of organic microlasers. PL spectra collected from an individual nanowire ($L =$ 70 nm) excited at different pump intensities.[132] Adapted with permission from ref. 132. Copyright 2020, Elsevier. (g) Fabrication of organic microwire optical vapor sensors. Fluorescence intensity variation plots exhibit similar organic vapors identification.[133] Adapted with permission from ref. 133. Copyright 2018, Springer Nature. (h) Scheme of the fabrication of organic 1D ultrathin crystals growing in the confined space. (i) Morphology tailoring induced by confined crystallization of organic ultrathin nanostructured arrays with different tunable shapes. (j) The thickness control of organic nanowires by tuning different pressures and solution concentrations.[134] Adapted with permission from ref. 134. Copyright 2019, Springer Nature.

remains free along the other two dimensions (Fig. 5h). By employing this nano-confined capillary bridge lithography method, we successfully realized the fabrication of ultrathin nanostructure arrays based on diversified solution-processable materials with the minimum height of 8.3 nm (five molecular layers of TIPS-pentacene) and programmable geometry, including circles, squares, pentagons and hexagons (Fig. 5i). To gain further insight into the fabrication of organic ultrathin nanowires controlled by pressure and the solution concentration, we performed the statistics of the average height of nanowires by tailoring the pressure ranging from 5.5 to 14 MPa and the concentration ranging from 1 to 5 mg mL^{-1} (Fig. 5j). We suppose that this nano-confined capillary bridge lithography method proves the feasibility of organic ultrathin architectures and opens up an opportunity to construct tunable and designable ultrathin organic nanostructures with high optoelectronic performance for organic integration circuits.

4. Conclusion and outlook

To date, impressive progress has been achieved in the areas of organic ultrathin nanostructures and organic crystal arrays from materials and methods to next-generation electronic/optoelectronic device applications. Decreasing the thickness of organic semiconductor crystals down to few or even monolayers provides the advantages of low contact resistance, and enhanced light response and gas sensing performance.[18] Currently, patterned organic semiconductor crystals have been successfully applied in high-integration devices such as FET arrays, logic circuits, active matrix displays and sensor arrays,[135,136] which can not only guarantee device uniformity and reproducibility, but can also reduce cross-talk between neighboring devices.[137] However, as a young and exciting research field, organic ultrathin arrays still present challenges and only have a few reports at present,[21,33,124,134,138,139] and are far from mature. For this, improvement of patterning strategies is urgent to prepare organic ultrathin arrays with precise alignment, high crystallinity and a tunable morphology.

As central building blocks of organic electronics, the development of FETs can create great potential for high-performance integrated devices. For organic ultrathin FET arrays, the reduced contact resistance and well-patterned organic semiconductor crystals provide opportunities for scaling down the devices. Meanwhile, low contact resistance can promise not only an accurate extraction of the mobility[140] but also a trustworthy study of the temperature-dependent FET performance.[141] In addition, the sensitivity of a sensor can be enhanced with decreasing the thickness of organic semiconductor crystals, and its response time can be simultaneously shortened.[138] This is because the ultrathin layer allows the direct contact of the accumulation region through external stimulation rather than diffusion. Thus, organic ultrathin FET arrays based on the integration of various organic semiconductor crystals are excellent platforms to improve the selectivity of gas analytes due to the interactions between gas analytes and different organic semiconductor crystals with unique characteristics.[142,143] Besides, organic semiconductor materials have the inherent advantage of compatibility with flexible substrates, and thin organic semiconductor crystals are desirable to reduce the bend-induced strain.[144] Therefore, organic ultrathin arrays are highly desirable for the application of next-generation wearable and retractable devices. Representative integrated devices have been successfully validated over the past few years due to the development of fabrication techniques, but these studies are still in their early stages.[21,139] First, for the assembly of ultrathin arrays, current strategies are limited to fabricate complex patterns towards integrated devices, which could only achieve ultrathin arrays with oriented alignment. Meanwhile, the manufacturing of ultrathin arrays with high-resolution, high-quality and controllable molecular-layer numbers remains a challenge. Consequently, greater effort should be expended to explore and develop new patterning technologies through one step. Typical methods of patterning organic ultrathin materials employ the "top–down" strategy, especially for the two-step fabrication methods of ultrathin arrays, which introduces an imprint method and photolithography to etch as-prepared ultrathin films with controllable molecular-layer numbers for fabricating organic ultrathin arrays.[21,139] Meanwhile, an in-depth understanding of crystallization kinetics and pathways is of paramount importance for the precise control of the assembly process. *In situ* techniques greatly promote the understanding of the crystallization mechanism, which can benefit the development of effective morphology control methods. Second, for applications, some issues in patterning organic ultrathin materials still need to be solved. (i) Due to relatively low physical or chemical stability, current organic ultrathin nanostructures generally lack long-term stability and durability. This can be achieved by developing more stable organic materials. (ii) At the present stage, the vast majority of applications rely on p-type organic materials; an enlarged material system is crucial for achieving multifunctional integrated devices. Therefore, further development of organic ultrathin integrated devices is to develop environmentally stable materials and practical methods for encapsulation, improve device processing technologies, optimize the device structure and explore the intrinsic mechanisms. Despite these challenges, given the sustained advances in large-scale and high-quality patterning and device fabrication techniques, the applications of organic ultrathin arrays in electronics and optoelectronics will have a bright future.

Conflicts of interest

There are no conflicts to declare.

Acknowledgements

This work was supported by the JiHua Laboratory Science Program (grant no. X190251UZ190), the Ministry of Science and Technology (MOST) of China (2017YFA0204504, 2018YFA0208502, and 2018YFA0704803), the National Natural Science Foundation (51922012 and 21633014) and the Youth Innovation Promotion Association CAS (2018034).

Notes and references

1 C. Wang, H. Dong, L. Jiang and W. Hu, *Chem. Soc. Rev.*, 2018, **47**, 422–500.
2 J. Nicks, K. Sasitharan, R. R. R. Prasad, D. J. Ashworth and J. A. Foster, *Adv. Funct. Mater.*, 2021, **31**, 2103723.
3 Y. Wang, L. Sun, C. Wang, F. Yang, X. Ren, X. Zhang, H. Dong and W. Hu, *Chem. Soc. Rev.*, 2019, **48**, 1492–1530.
4 Y. L. Shi and X. D. Wang, *Adv. Funct. Mater.*, 2020, **31**, 2008149.
5 H. Lai and F. He, *Adv. Energy Mater.*, 2020, **10**, 2002678.
6 Q. Y. Li, Z. F. Yao, J. Y. Wang and J. Pei, *Rep. Prog. Phys.*, 2021, **84**, 076601.
7 S. Chong, D. T. Park and J. Kim, *J. Phys. Chem. C*, 2021, **125**, 10198–10206.
8 M. Singh, K. Liu, S. Qu, H. Ma, H. Shi, Z. An and W. Huang, *Adv. Opt. Mater.*, 2021, **9**, 2002197.
9 Y. Quan, G. Lan, Y. Fan, W. Shi, E. You and W. Lin, *J. Am. Chem. Soc.*, 2020, **142**, 1746–1751.

10 P. Yu, Y. Zhen, H. Dong and W. Hu, *Chem*, 2019, **5**, 2814–2853.
11 C. Tan, X. Cao, X. J. Wu, Q. He, J. Yang, X. Zhang, J. Chen, W. Zhao, S. Han, G. H. Nam, M. Sindoro and H. Zhang, *Chem. Rev.*, 2017, **117**, 6225–6331.
12 P. K. L. Chan, *Adv. Electron. Mater.*, 2019, **5**, 1900029.
13 F. Yang, S. Cheng, X. Zhang, X. Ren, R. Li, H. Dong and W. Hu, *Adv. Mater.*, 2018, **30**, 1702415.
14 H. Zhang, *ACS Nano*, 2015, **10**, 9451–9469.
15 S. Hu and M. Zhu, *ChemCatChem*, 2019, **11**, 6147–6165.
16 M. Chu, J. X. Fan, S. Yang, D. Liu, C. F. Ng, H. Dong, A. M. Ren and Q. Miao, *Adv. Mater.*, 2018, **30**, 1803467.
17 H. Minemawari, T. Yamada, H. Matsui, J. Tsutsumi, S. Haas, R. Chiba, R. Kumai and T. Hasegawa, *Nature*, 2011, **475**, 364–367.
18 Y. W. Fan, J. Liu, W. P. Hu, Y. Q. Liu and L. Jiang, *J. Mater. Chem. C*, 2020, **8**, 13154–13168.
19 H. Klauk, *Adv. Electron. Mater.*, 2018, **4**, 1700474.
20 J. G. Feng, C. Gong, H. F. Gao, W. Wen, Y. J. Gong, X. Y. Jiang, B. Zhang, Y. C. Wu, Y. S. Wu, H. B. Fu, L. Jiang and X. Zhang, *Nat. Electron.*, 2018, **1**, 404–410.
21 S. Duan, T. Wang, B. Geng, X. Gao, C. Li, J. Zhang, Y. Xi, X. Zhang, X. Ren and W. Hu, *Adv. Mater.*, 2020, **32**, 1908388.
22 J. G. Feng, W. Wen, X. Wei, X. Y. Jiang, M. Y. Cao, X. D. Wang, X. Q. Zhang, L. Jiang and Y. C. Wu, *Adv. Mater.*, 2019, **31**, 1807880.
23 Z. Chen, S. Duan, X. Zhang and W. Hu, *Appl. Phys. Lett.*, 2021, **119**, 040501.
24 Z. Lu, C. Wang, W. Deng, M. T. Achille, J. Jie and X. Zhang, *J. Mater. Chem. C*, 2020, **8**, 9133–9146.
25 R. A. Nawrocki, *Adv. Funct. Mater.*, 2019, **29**, 1906908.
26 P. Kissel, R. Erni, W. B. Schweizer, M. D. Rossell, B. T. King, T. Bauer, S. Gotzinger, A. D. Schluter and J. Sakamoto, *Nat. Chem.*, 2012, **4**, 287–291.
27 A. C. Grimsdale, K. L. Chan, R. E. Martin, P. G. Jokisz and A. B. Holmes, *Chem. Rev.*, 2009, **109**, 897–1091.
28 L. Z. Huang, X. R. Hu and L. F. Chi, *Langmuir*, 2015, **31**, 9748–9761.
29 Y. Yang, K. Mielczarek, M. Aryal, A. Zakhidov and W. Hu, *ACS Nano*, 2012, **6**, 2877–2892.
30 L. Q. Li, P. Gao, M. Baumgarten, K. Mullen, N. Lu, H. Fuchs and L. F. Chi, *Adv. Mater.*, 2013, **25**, 3419–3425.
31 J. L. Segura, M. J. Mancheno and F. Zamora, *Chem. Soc. Rev.*, 2016, **45**, 5635–5671.
32 S. Z. Yang, W. H. Hu, X. Zhang, P. L. He, B. Pattengale, C. M. Liu, M. Cendejas, I. Hermans, X. Y. Zhang, J. Zhang and J. E. Huang, *J. Am. Chem. Soc.*, 2018, **140**, 14614–14618.
33 J. J. Duan, S. Chen and C. Zhao, *Nat. Commun.*, 2017, **8**, 15341.
34 M. Q. Huang, W. W. Liu, L. Wang, J. W. Liu, G. Y. Chen, W. B. You, J. Zhang, L. J. Yuan, X. F. Zhang and R. C. Che, *Nano Res.*, 2020, **13**, 810–817.
35 Y. F. Xu, M. G. Schwab, A. J. Strudwick, I. Hennig, X. L. Feng, Z. S. Wu and K. Mullen, *Adv. Energy Mater.*, 2013, **3**, 1035–1040.
36 S. Chen, Z. Li, Y. Qiao and Y. Song, *J. Mater. Chem. C*, 2021, **9**, 1126–1149.
37 J. L. Zhang, S. Zhong, J. Q. Zhong, T. C. Niu, W. P. Hu, A. T. Wee and W. Chen, *Nanoscale*, 2015, **7**, 4306–4324.
38 Y. Diao, L. Shaw, Z. Bao and S. C. B. Mannsfeld, *Energy Environ. Sci.*, 2014, **7**, 2145–2159.
39 M. Cao, C. Zhang, Z. Cai, C. Xiao, X. Chen, K. Yi, Y. Yang, Y. Lu and D. Wei, *Nat. Commun.*, 2019, **10**, 756.
40 X. Liu, X. Luo, H. Nan, H. Guo, P. Wang, L. Zhang, M. Zhou, Z. Yang, Y. Shi, W. Hu, Z. Ni, T. Qiu, Z. Yu, J. B. Xu and X. Wang, *Adv. Mater.*, 2016, **28**, 5200–5205.
41 D. He, Y. Zhang, Q. Wu, R. Xu, H. Nan, J. Liu, J. Yao, Z. Wang, S. Yuan, Y. Li, Y. Shi, J. Wang, Z. Ni, L. He, F. Miao, F. Song, H. Xu, K. Watanabe, T. Taniguchi, J. B. Xu and X. Wang, *Nat. Commun.*, 2014, **5**, 5162.
42 B. Wu, Y. Zhao, H. Nan, Z. Yang, Y. Zhang, H. Zhao, D. He, Z. Jiang, X. Liu, Y. Li, Y. Shi, Z. Ni, J. Wang, J. B. Xu and X. Wang, *Nano Lett.*, 2016, **16**, 3754–3759.
43 C. Xu, P. He, J. Liu, A. Cui, H. Dong, Y. Zhen, W. Chen and W. Hu, *Angew. Chem.*, 2016, **55**, 9519–9523.
44 C. Wang, X. Ren, C. Xu, B. Fu, R. Wang, X. Zhang, R. Li, H. Li, H. Dong, Y. Zhen, S. Lei, L. Jiang and W. Hu, *Adv. Mater.*, 2018, **30**, 1706260.
45 X. Zhu, Y. Zhang, X. Ren, J. Yao, S. Guo, L. Zhang, D. Wang, G. Wang, X. Zhang, R. Li and W. Hu, *Small*, 2019, **15**, 1902187.
46 J. Yao, Y. Zhang, X. Tian, X. Zhang, H. Zhao, X. Zhang, J. Jie, X. Wang, R. Li and W. Hu, *Angew. Chem., Int. Ed.*, 2019, **58**, 16082–16086.
47 Q. Wang, J. Qian, Y. Li, Y. Zhang, D. He, S. Jiang, Y. Wang, X. Wang, L. Pan, J. Wang, X. Wang, Z. Hu, H. Nan, Z. Ni, Y. Zheng and Y. Shi, *Adv. Funct. Mater.*, 2016, **26**, 3191–3198.
48 M. K. Lee, M. Shokouhimehr, S. Y. Kim and H. W. Jang, *Adv. Energy Mater.*, 2021, **12**, 2003990.
49 K. Liu, L. Wang and R. Dong, *J. Mater. Chem. C*, 2020, **8**, 10696–10718.
50 P. Wang, Y. Peng, C. Zhu, R. Yao, H. Song, L. Kun and W. Yang, *Angew. Chem., Int. Ed.*, 2021, **60**, 19047–19052.
51 X. Shi, D. Ma, F. Xu, Z. Zhang and Y. Wang, *Chem. Sci.*, 2020, **11**, 989–996.
52 L. Grill, M. Dyer, L. Lafferentz, M. Persson, M. V. Peters and S. Hecht, *Nat. Nanotechnol.*, 2007, **2**, 687–691.
53 L. Lafferentz, V. Eberhardt, C. Dri, C. Africh, G. Comelli, F. Esch, S. Hecht and L. Grill, *Nat. Chem.*, 2012, **4**, 215–220.
54 H. Wang, Q. Jiang, J. Yang, D. Li, X. Zhou, L. Cai and G. Yu, *Adv. Mater. Interfaces*, 2020, **7**, 2000979.
55 K. Liu, H. Qi, R. Dong, R. Shivhare, M. Addicoat, T. Zhang, H. Sahabudeen, T. Heine, S. Mannsfeld, U. Kaiser, Z. Zheng and X. Feng, *Nat. Chem.*, 2019, **11**, 994–1000.
56 S. Park, Z. Liao, B. Ibarlucea, H. Qi, H. H. Lin, D. Becker, J. Melidonie, T. Zhang, H. Sahabudeen, L. Baraban, C. K. Baek, Z. Zheng, E. Zschech, A. Fery, T. Heine, U. Kaiser, G. Cuniberti, R. Dong and X. Feng, *Angew. Chem., Int. Ed.*, 2020, **59**, 8218–8224.
57 H. Sahabudeen, H. Qi, M. Ballabio, M. Polozij, S. Olthof, R. Shivhare, Y. Jing, S. Park, K. Liu, T. Zhang, J. Ma, B. Rellinghaus, S. Mannsfeld, T. Heine, M. Bonn, E. Canovas, Z. Zheng, U. Kaiser, R. Dong and X. Feng, *Angew. Chem., Int. Ed.*, 2020, **59**, 6028–6036.

58 C. Li, Y. Wang, Y. Zou, X. Zhang, H. Dong and W. Hu, *Angew. Chem., Int. Ed.*, 2020, **59**, 9403–9407.
59 Y. Li, M. Zhang, X. Guo, R. Wen, X. Li, X. Li, S. Li and L. Ma, *Nanoscale Horiz.*, 2018, **3**, 205–212.
60 M. Zhao, Y. Wang, Q. Ma, Y. Huang, X. Zhang, J. Ping, Z. Zhang, Q. Lu, Y. Yu, H. Xu, Y. Zhao and H. Zhang, *Adv. Mater.*, 2015, **27**, 7372–7378.
61 S. Zhao, Y. Wang, J. Dong, C.-T. He, H. Yin, P. An, K. Zhao, X. Zhang, C. Gao, L. Zhang, J. Lv, J. Wang, J. Zhang, A. M. Khattak, N. A. Khan, Z. Wei, J. Zhang, S. Liu, H. Zhao and Z. Tang, *Nat. Energy*, 2016, **1**, 16184–16194.
62 P. Zhao, M. Jian, Q. Zhang, R. Xu, R. Liu, X. Zhang and H. Liu, *J. Mater. Chem. A*, 2019, **7**, 16598–16621.
63 C. Tan, G. Liu, H. Li, Y. Cui and Y. Liu, *Dalton Trans.*, 2020, **49**, 11073–11084.
64 Y. Fan, J. Zhang, Y. Shen, B. Zheng, W. Zhang and F. Huo, *Nano Res.*, 2020, **14**, 1–28.
65 C. Zhang, B. H. Wu, M. Q. Ma, Z. Wang and Z. K. Xu, *Chem. Soc. Rev.*, 2019, **48**, 3811–3841.
66 Y. Zheng, F. Z. Sun, X. Han, J. Xu and X. H. Bu, *Adv. Opt. Mater.*, 2020, **8**, 2000110.
67 I. Stassen, J. H. Dou, C. Hendon and M. Dinca, *ACS Cent. Sci.*, 2019, **5**, 1425–1431.
68 Z. Qiao, Y. Liang, Z. Zhang, D. Mei, Z. Wang, M. D. Guiver and C. Zhong, *Adv. Mater.*, 2020, **32**, 2002165.
69 A. Dhakshinamoorthy, A. M. Asiri and H. Garcia, *Adv. Mater.*, 2019, **31**, 1900617.
70 B. J. Cordova Wong, D. M. Xu, S. S. Bao, L. M. Zheng and J. Lei, *ACS Appl. Mater. Interfaces*, 2019, **11**, 12986–12992.
71 G. Grancini and M. K. Nazeeruddin, *Nat. Rev. Mater.*, 2018, **4**, 4–22.
72 Y. Fu, H. Zhu, J. Chen, M. P. Hautzinger, X. Y. Zhu and S. Jin, *Nat. Rev. Mater.*, 2019, **4**, 169–188.
73 L. Etgar, *Energy Environ. Sci.*, 2018, **11**, 234–242.
74 L. N. Quan, M. Yuan, R. Comin, O. Voznyy, E. M. Beauregard, S. Hoogland, A. Buin, A. R. Kirmani, K. Zhao, A. Amassian, D. H. Kim and E. H. Sargent, *J. Am. Chem. Soc.*, 2016, **138**, 2649–2655.
75 J. Liu, Y. Xue, Z. Wang, Z. Q. Xu, C. Zheng, B. Weber, J. Song, Y. Wang, Y. Lu, Y. Zhang and Q. Bao, *ACS Nano*, 2016, **10**, 3536–3542.
76 S. Yang, W. Niu, A. L. Wang, Z. Fan, B. Chen, C. Tan, Q. Lu and H. Zhang, *Angew. Chem., Int. Ed.*, 2017, **56**, 4252–4255.
77 K. Leng, I. Abdelwahab, I. Verzhbitskiy, M. Telychko, L. Chu, W. Fu, X. Chi, N. Guo, Z. Chen, Z. Chen, C. Zhang, Q. H. Xu, J. Lu, M. Chhowalla, G. Eda and K. P. Loh, *Nat. Mater.*, 2018, **17**, 908–914.
78 K. Y. Kim, G. Park, J. Cho, J. Kim, J. S. Kim, J. Jung, K. Park, C. Y. You and I. H. Oh, *Small*, 2020, **16**, 2005445.
79 L. T. Dou, A. B. Wong, Y. Yu, M. L. Lai, N. Kornienko, S. W. Eaton, A. Fu, C. G. Bischak, J. Ma, T. N. Ding, N. S. Ginsberg, L. W. Wang, A. P. Alivisatos and P. D. Yang, *Science*, 2015, **349**, 1518–1521.
80 K. Leng, W. Fu, Y. Liu, M. Chhowalla and K. P. Loh, *Nat. Rev. Mater.*, 2020, **5**, 482–500.
81 X. Fu, S. Jiao, Y. Jiang, L. Li, X. Wang, C. Zhu, C. Ma, H. Zhao, Z. Xu, Y. Liu, W. Huang, W. Zheng, P. Fan, F. Jiang, D. Zhang, X. Zhu, X. Wang and A. Pan, *ACS Appl. Mater. Interfaces*, 2020, **12**, 2884–2891.
82 Y. B. Guo, L. Xu, H. B. Liu, Y. J. Li, C. M. Che and Y. L. Li, *Adv. Mater.*, 2015, **27**, 985–1013.
83 J. P. Meng and Z. Li, *Adv. Mater.*, 2020, **32**, 2000130.
84 Q. Tang, H. Li, Y. Song, W. Xu, W. Hu, L. Jiang, Y. Liu, X. Wang and D. Zhu, *Adv. Mater.*, 2006, **18**, 3010–3014.
85 W. Wang, C. Du, D. Zhong, M. Hirtz, Y. Wang, N. Lu, L. Wu, D. Ebeling, L. Li, H. Fuchs and L. Chi, *Adv. Mater.*, 2009, **21**, 4721–4725.
86 Z. Fang, H. Wang, J. Liang, Z. Wang, W. Wang and F. Huang, *Adv. Mater. Technol.*, 2022, 2101457, DOI: 10.1002/admt.202101457.
87 Y. Wu, J. Feng, X. Jiang, Z. Zhang, X. Wang, B. Su and L. Jiang, *Nat. Commun.*, 2015, **6**, 6737.
88 H. Li, B. C. Tee, J. J. Cha, Y. Cui, J. W. Chung, S. Y. Lee and Z. Bao, *J. Am. Chem. Soc.*, 2012, **134**, 2760–2765.
89 H. Li, B. C. Tee, G. Giri, J. W. Chung, S. Y. Lee and Z. Bao, *Adv. Mater.*, 2012, **24**, 2588–2591.
90 G. Xue, C. Fan, J. Wu, S. Liu, Y. Liu, H. Chen, H. L. Xin and H. Li, *Mater. Horiz.*, 2015, **2**, 344–349.
91 C. T. Hsieh, C. Y. Chen, H. Y. Lin, C. J. Yang, T. J. Chen, K. Y. Wu and C. L. Wang, *J. Phys. Chem. C*, 2018, **122**, 16242–16248.
92 G. Mattana, A. Loi, M. Woytasik, M. Barbaro, V. Noël and B. Piro, *Adv. Mater. Technol.*, 2017, **2**, 1700063.
93 N. Mizoshita, Y. Yamada, M. Murase, Y. Goto and S. Inagaki, *Nanoscale*, 2020, **12**, 21146–21154.
94 W. B. Jung, S. Jang, S. Y. Cho, H. J. Jeon and H. T. Jung, *Adv. Mater.*, 2020, **32**, 1907101.
95 H. Ma, Z. Jiang, X. Xie, L. Huang and W. Huang, *ACS Appl. Mater. Interfaces*, 2018, **10**, 25121–25126.
96 Z. Q. Li, P. Guo and Y. G. Zhou, *Adv. Mater. Technol.*, 2021, **6**, 2000897.
97 R. Bian, L. Meng, M. Zhang, L. Chen and H. Liu, *ACS Omega*, 2019, **4**, 1816–1823.
98 K. Motai, T. Narimatsu, C. Chen and Y. Hayamizu, *J. Mater. Chem. C*, 2020, **8**, 8585–8591.
99 J. G. Feng, X. Y. Jiang, X. X. Yan, Y. C. Wu, B. Su, H. B. Fu, J. N. Yao and L. Jiang, *Adv. Mater.*, 2017, **29**, 1603652.
100 Y. C. Wu, J. G. Feng, H. F. Gao, X. J. Feng and L. Jiang, *Adv. Mater.*, 2019, **31**, 1800718.
101 M. Gao, L. Li and Y. Song, *J. Mater. Chem. C*, 2017, **5**, 2971–2993.
102 C. H. Lin, C. Y. Kang, T. Z. Wu, C. L. Tsai, C. W. Sher, X. Guan, P. T. Lee, T. Wu, C. H. Ho, H. C. Kuo and J. H. He, *Adv. Funct. Mater.*, 2020, **30**, 1909275.
103 L. Shi, L. Meng, F. Jiang, Y. Ge, F. Li, X. g. Wu and H. Zhong, *Adv. Funct. Mater.*, 2019, **29**, 1903648.
104 D. Li, J. Wang, M. Li, G. Xie, B. Guo, L. Mu, H. Li, J. Wang, H. L. Yip and J. Peng, *Adv. Mater. Technol.*, 2020, **5**, 2000099.
105 X. Fang, J. Shi, X. Zhang, X. Ren, B. Lu, W. Deng, J. Jie and X. Zhang, *Adv. Funct. Mater.*, 2021, **31**, 2100237.
106 J. Yang, J. Yoo, W. S. Yu and M. K. Choi, *Macromol. Res.*, 2021, **29**, 391–401.
107 V. Suresh, L. Ding, A. B. Chew and F. L. Yap, *ACS Appl. Nano Mater.*, 2018, **1**, 886–893.

108 M. F. Shahin Shahidan, J. Song, T. D. James and A. Roberts, *Nanoscale Adv.*, 2020, **2**, 2177–2184.
109 J. Ge, B. Ding, S. Hou, M. Luo, D. Nam, H. Duan, H. Gao, Y. C. Lam and H. Li, *Nat. Commun.*, 2021, **12**, 3146.
110 J. Oh, J. B. Hoffman, S. Hong, K. D. Jo, J. Roman-Kustas, J. H. Reed, C. E. Dana, D. M. Cropek, M. Alleyne and N. Miljkovic, *Nano Lett.*, 2020, **20**, 6989–6997.
111 H. Zhang, Q. Liao, Y. Wu, Z. Zhang, Q. Gao, P. Liu, M. Li, J. Yao and H. Fu, *Adv. Mater.*, 2018, **30**, 1706186.
112 R. D. Piner, J. Zhu, F. Xu, S. Hong and C. A. Mirkin, *Science*, 1999, **283**, 661–663.
113 G. Liu, M. Hirtz, H. Fuchs and Z. Zheng, *Small*, 2019, **15**, 1900564.
114 G. Liu, S. H. Petrosko, Z. Zheng and C. A. Mirkin, *Chem. Rev.*, 2020, **120**, 6009–6047.
115 S. Zhu, Y. Tang, C. Lin, X. Y. Liu and Y. Lin, *Small Methods*, 2021, **5**, 2001060.
116 R. Kumar, A. Urtizberea, S. Ghosh, U. Bog, Q. Rainer, S. Lenhert, H. Fuchs and M. Hirtz, *Langmuir*, 2017, **33**, 8739–8748.
117 J. P. Agusil, N. Torras, M. Duch, J. Esteve, L. Pérez-García, J. Samitier and J. A. Plaza, *Adv. Funct. Mater.*, 2017, **27**, 1605912.
118 J. S. Du, D. Shin, T. K. Stanev, C. Musumeci, Z. Xie, Z. Huang, M. Lai, L. Sun, W. Zhou, N. P. Stern, V. P. Dravid and C. A. Mirkin, *Sci. Adv.*, 2020, **6**, eabc4959.
119 G. Giri, E. Verploegen, S. C. Mannsfeld, S. Atahan-Evrenk, D. H. Kim, S. Y. Lee, H. A. Becerril, A. Aspuru-Guzik, M. F. Toney and Z. Bao, *Nature*, 2011, **480**, 504–508.
120 Y. Diao, B. C. Tee, G. Giri, J. Xu, D. H. Kim, H. A. Becerril, R. M. Stoltenberg, T. H. Lee, G. Xue, S. C. Mannsfeld and Z. Bao, *Nat. Mater.*, 2013, **12**, 665–671.
121 D. Khim, A. Luzio, G. E. Bonacchini, G. Pace, M. J. Lee, Y. Y. Noh and M. Caironi, *Adv. Mater.*, 2018, **30**, 1705463.
122 M. Pandey, N. Kumari, S. Nagamatsu and S. S. Pandey, *J. Mater. Chem. C*, 2019, **7**, 13323–13351.
123 J. Shin, T. R. Hong, T. W. Lee, A. Kim, Y. H. Kim, M. J. Cho and D. H. Choi, *Adv. Mater.*, 2014, **26**, 6031–6035.
124 J. O. Kim, J. C. Lee, M. J. Kim, H. Noh, H. I. Yeom, J. B. Ko, T. H. Lee, S. H. Ko Park, D. P. Kim and S. Park, *Adv. Mater.*, 2018, **30**, 1800647.
125 H. F. Gao, J. G. Feng, B. Zhang, C. Y. Xiao, Y. C. Wu, X. N. Kan, B. Su, Z. H. Wang, W. P. Hu, Y. M. Sun, L. Jiang and A. J. Heeger, *Adv. Funct. Mater.*, 2017, **27**, 1701347.
126 X. Wei, H. F. Gao, J. G. Feng, Y. Y. Pi, B. Zhang, Y. Zhai, W. Wen, M. Q. He, J. R. Matthews, H. X. Wang, Y. Li, S. M. Jiang, L. Jiang and Y. C. Wu, *ACS Appl. Mater. Interfaces*, 2019, **11**, 15829–15836.
127 Y. J. Zhao, Y. C. Qiu, H. F. Gao, J. G. Feng, G. S. Chen, L. Jiang and Y. C. Wu, *Adv. Mater.*, 2020, **32**, 1905298.
128 G. S. Chen, Y. C. Qiu, H. F. Gao, Y. J. Zhao, J. G. Feng, L. Jiang and Y. C. Wu, *Adv. Funct. Mater.*, 2020, **30**, 1908894.
129 J. G. Feng, Q. Song, B. Zhang, Y. C. Wu, T. Wang and L. Jiang, *Adv. Mater.*, 2017, **29**, 1703143.
130 B. Zhang, F. S. Meng, J. G. Feng, J. X. Wang, Y. C. Wu and L. Jiang, *Adv. Mater.*, 2018, **30**, 1707291.
131 Y. J. Zhao, Y. C. Qiu, J. G. Feng, J. H. Zhao, G. S. Chen, H. F. Gao, Y. Y. Zhao, L. Jiang and Y. C. Wu, *J. Am. Chem. Soc.*, 2021, **143**, 8437–8445.
132 J. J. Wu, H. F. Gao, R. C. Lai, M. P. Zhuo, J. G. Feng, X. D. Wang, Y. C. Wu, L. S. Liao and L. Jiang, *Matter*, 2020, **2**, 1233–1243.
133 X. Y. Jiang, H. F. Gao, X. Q. Zhang, J. H. Pang, Y. Q. Li, K. Li, Y. C. Wu, S. Z. Li, J. Zhu, Y. Wei and L. Jiang, *Nat. Commun.*, 2018, **9**, 3799.
134 H. F. Gao, Y. C. Qiu, J. G. Feng, S. Li, H. J. Wang, Y. Y. Zhao, X. Wei, X. Y. Jiang, Y. W. Su, Y. C. Wu and L. Jiang, *Nat. Commun.*, 2019, **10**, 3912.
135 X. Zhang, W. Deng, R. Jia, X. Zhang and J. Jie, *Small*, 2019, **15**, 1900332.
136 W. Deng, X. J. Zhang, H. L. Dong, J. S. Jie, X. Z. Xu, J. Liu, L. He, L. Xu, W. P. Hu and X. H. Zhang, *Mater. Today*, 2019, **4**, 17–25.
137 X. Zhang, J. Jie, W. Deng, Q. Shang, J. Wang, H. Wang, X. Chen and X. Zhang, *Adv. Mater.*, 2016, **28**, 2475–2503.
138 H. Yang, M. Su, K. Li, L. Jiang, Y. Song, M. Doi and J. Wang, *Langmuir*, 2014, **30**, 9436–9441.
139 Z. Chen, S. Duan, X. Zhang, B. Geng, Y. Xiao, J. Jie, H. Dong, L. Li and W. Hu, *Adv. Mater.*, 2021, 2104166.
140 C. Liu, G. Li, R. Di Pietro, J. Huang, Y. Y. Noh, X. Liu and T. Minari, *Phys. Rev. Appl.*, 2017, **8**, 034020.
141 Y. Hu, G. Li and Z. Chen, *IEEE Electron Device Lett.*, 2018, **39**, 276–279.
142 B. Crone, A. Dodabalapur, A. Gelperin, L. Torsi, H. E. Katz, A. J. Lovinger and Z. Bao, *Appl. Phys. Lett.*, 2001, **78**, 2229–2231.
143 W. Huang, J. Sinha, M. L. Yeh, J. F. M. Hardigree, R. LeCover, K. Besar, A. M. Rule, P. N. Breysse and H. E. Katz, *Adv. Funct. Mater.*, 2013, **23**, 4094–4104.
144 H. T. Yi, M. M. Payne, J. E. Anthony and V. Podzorov, *Nat. Commun.*, 2012, **3**, 1259.